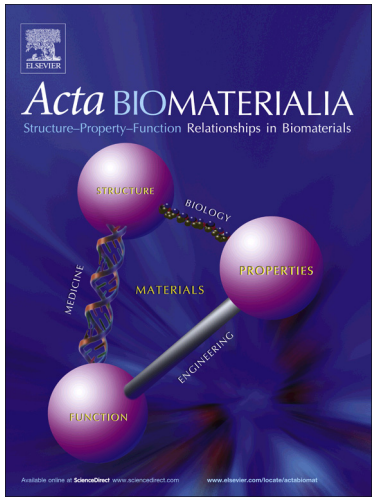

Lectin-Conjugated pH-Responsive Mesoporous Silica Nanoparticles for Targeted Bone Cancer Treatment

Marina Martínez-Carmona, Daniel Lozano, Montserrat Colilla, María Vallet-Regí

PII: S1742-7061(17)30692-X
DOI: https://doi.org/10.1016/j.actbio.2017.11.007
Reference: ACTBIO 5160

To appear in: *Acta Biomaterialia*

Received Date: 28 July 2017
Revised Date: 7 October 2017
Accepted Date: 7 November 2017

Please cite this article as: Martínez-Carmona, M., Lozano, D., Colilla, M., Vallet-Regí, M., Lectin-Conjugated pH-Responsive Mesoporous Silica Nanoparticles for Targeted Bone Cancer Treatment, *Acta Biomaterialia* (2017), doi: https://doi.org/10.1016/j.actbio.2017.11.007

Manuscript submitted to

Acta Biomaterialia

October 2017

(Revised Version)

Lectin-Conjugated pH-Responsive Mesoporous Silica Nanoparticles for Targeted Bone Cancer Treatment

Marina Martínez-Carmona,[a,b] Daniel Lozano,[a,b] Montserrat Colilla,[a,b*]

María Vallet-Regí[a,b*]

[a] Dpto. Química Inorgánica y Bioinorgánica Universidad Complutense de Madrid. Instituto de Investigación Sanitaria Hospital 12 de Octubre i+12. Plaza Ramón y Cajal s/n, 28040 Madrid, Spain.

[b] CIBER de Bioingeniería, Biomateriales y Nanomedicina, CIBER-BBN, Madrid, Spain.

[*] Corresponding authors: Fax: +34 394 1786; Tel.: +34 91 394 1843; E-mail addresses: vallet@ucm.es (M. Vallet-Regí) and mcolilla@ucm.es (M. Colilla)

Abstract

A novel multifunctional nanodevice based in doxorubicin (DOX)-loaded mesoporous silica nanoparticles (MSNs) as nanoplatforms for the assembly of different building blocks has been developed for bone cancer treatment. These building blocks consists of: i) a polyacrylic acid (PAA) capping layer grafted to MSNs *via* an acid-cleavable acetal linker, to minimize premature cargo release and provide the nanosystem of pH-responsive drug delivery ability; and ii) a targeting ligand, the plant lectin concanavalin A (ConA), able to selectively recognize, bind and internalize owing to certain cell-surface glycans, such as sialic acids (SA), overexpressed in given tumor cells. This multifunctional nanosystem exhibits a noticeable higher internalization degree into human osteosarcoma cells (HOS), overexpressing SA, compared to healthy preosteoblast cells (MC3T3-E1). Moreover, the results indicate that small DOX loading (2.5 μg mL^{-1}) leads to almost 100% of osteosarcoma cell death in comparison with healthy bone cells, which significantly preserve their viability. Besides, this nanodevice has a cytotoxicity on tumor cells 8-fold higher than that caused by the free drug. These findings demonstrate that the synergistic combination of different building blocks into a unique nanoplatform increases antitumor effectiveness and decreases toxicity towards normal cells. This line of attack opens up new insights in targeted bone cancer therapy.

STATEMENT OF SIGNIFICANCE

The development of highly selective and efficient tumor-targeted smart drug delivery nanodevices remains a great challenge in nanomedicine. This work reports the design and optimization of a multifunctional nanosystem based on mesoporous silica nanoparticles (MSNs) featuring selectivity towards human osteosarcoma cells and pH-responsive antitumor drug delivery capability. The novelty and originality of this manuscript relies on proving that the synergistic assembly of different building blocks into a unique nanoplatform increases antitumor effectiveness and decreases toxicity towards healthy cells, which constitutes a new paradigm in targeted bone cancer therapy.

Keywords

Antitumor Effect; Bone Cancer; Lectin; Mesoporous Silica Nanoparticles; Nanomedicine; pH-Responsive Drug Release; Synergistic Combination; Targeting.

1. Introduction

The major constraint of conventional chemotherapy for cancer treatment is the lack of specificity of cytotoxic drugs. This constitutes a serious threat to healthy tissues, resulting in a significant decrease of the efficacy and provoking the apparition of side-effects in the patient associated to systemic toxicity[1]. The emergence of nanotechnology has transformed this scenario owing to the development of nanocarriers for therapeutic agents[2]. Particularly, in the last two decades much research effort has been devoted to build nanocarriers for tumor-targeted stimuli-responsive drug delivery[3-7].

Among nanocarriers, mesoporous silica nanoparticles (MSNs) are receiving growing interest since they exhibit unique properties such as large surface areas and pore volumes, which provide high loading capability, customized sizes, morphology and pore diameters, robustness and easy functionalization[8-19]. Moreover, they exhibit low cytotoxicity[20] and good hemocompatibility[21]. These features provide exceptional opportunities to host different therapeutic payloads. Hence, the tunable surface of MSNs chemistry allows the attachment of organic functionalities such as pore blocking agents to avoid premature cargo release, or targeting ligands to guide MSNs towards diseased tissues.

In this sense, during the last few years, a wide range of stimuli-responsive drug delivery systems, achieving release profiles with spatial, temporal and dosage control have been reported[4,15,17]. The performance of these smart nanosystems relies on triggering drug release at the target site by using moieties that are sensitive to external stimuli (light, magnetic fields, electric fields, ultrasounds, etc.)[22-30], internal stimuli (variations in pH, redox potential, or the concentrations of enzymes or specific analytes)[31-36], or combination of both[37]. However, the side effects in

most of these nanosystems cannot be disregarded in practice because these particles frequently lack of specific cancer cell targeting capability and can be also internalized by normal cells. In the last decade, considerable research effort has been committed to develop tumor-targeted stimuli-responsive drug delivery systems. Although diverse targeting ligands, such as transferrin[23,35,38], certain peptides[39], hyaluronic acid[40,41], or folic acid[31,42], have been incorporated into stimuli-responsive MSNs, the development of highly selective and efficient tumor-targeted smart drug delivery nanodevices remains a tremendous challenge. Among the different antitumor drugs, doxorubicin (DOX) is receiving great attention because it is commonly used in the treatment of many types of cancer [43], including osteosarcoma bone tumors [44]. In this sense, much research effort is being devoted to design smart DOX-loaded MSNs aimed at overcoming the main limitation of conventional administered DOX in chemotherapy, *i.e.* its significant systemic toxicity [23,45-51]. However, to the best of our knowledge, none of them incorporates stimuli-responsive DOX release and targeting elements to distinguish between healthy and tumor bone cells for the efficient development of targeted bone cancer therapies.

Herein we have designed and developed a multifunctional nanodevice based in DOX-loaded MSNs acting as nanoplatforms for the assembly of different building blocks: i) a pH-sensitive layer consisting in polyacrylic acid (PAA) anchored to the MSNs surface *via* an acid-cleavable acetal linker.[52].PAA was used as pore blocking agent due to its good properties such as biocompatibility, hydrophilicity and abundance of carboxylic groups prone to experience easy functionalization[53]; and ii) a targeting ligand, the lectin concanavalin A (ConA) grafted to PAA, to increase the selectivity of the nanocarrier towards cancer cells and preserve the viability of healthy cells. ConA was chosen as targeting ligand owing the capability of this plant lectin to selectively recognize and bind to cell-surface glycans, which are frequently overexpressed in cancer cells[54,55].

The pH-responsive drug delivery performance of the nanosystem was evaluated “in vial” using $[Ru(bipy)_3]^{2+}$ as model molecule. The results demonstrate that in acidic conditions (pH 5.3) mimicking those of endo/lysosomes drug released is faster than in physiological conditions (pH 7.4). Then, the capacity of this multifunctional nanodevice to selectively eradicate human

osteosarcoma cancer cells (HOS), overexpressing sialic acid (SA) glycans as ConA receptors, compared to healthy preosteoblastic cells (MC3T3-E1), non-overexpressing SA, was *in vitro* evaluated. The results indicate the preferential internalization of the nanosystems into tumor cells and that only very small DOX concentrations are needed to almost completely eradicate osteosarcoma cells meanwhile preserving the viability of healthy bone cells. This resulted in a 100% killing efficacy against tumor cells in comparison with normal cells, as well as 8-fold higher tumor cytotoxicity than that caused by free DOX. We envision this novel multifunctional nanodevice as a potential candidate to be incorporated into a nanomedicines library for targeted bone cancer therapy.

2. Materials and Methods

2.1 Reagents

Tetraethylorthosilicate (TEOS, 98%), n-cetyltrimethylammo-nium bromide (CTAB, ≥ 99%), sodium hydroxide (NaOH, ≥ 98%), ammonium nitrate (NH_4NO_3, ≥ 98%), sodium carbonate (Na_2CO_3, ≥ 99,5%), hydrochloric acid (HCl, 37%), fluorescein 5(6)-isothiocyanate (FITC, ≥ 98%), (3-aminopropyl) triethoxysilane (APTES, ≥ 98%), N-(3-Dimethylaminopropyl)-N′-ethylcarbodiimide hydrochloride (EDC, ≥ 98%), N-Hydroxysulfosuccinimide sodium salt (sulfo-NHS, ≥ 98%), poly(acrylic acid) partial sodium salt solution (PAA, average Mw ~ 240,000 by GPC, 25 wt.% in H_2O), phosphate-buffered saline (PBS, 10x), phosphotungstic acid hydrate (PTA, reagent grade), Concanavalin A from Canavalia ensiformis (Jack bean) (ConA, Type VI lyophilized powder), tris(bipyridine)ruthenium(II) chloride ($[Ru(bipy)_3]Cl_2$), and doxorubicin hydrochloride (DOX, European Pharmacopoeia) were purchased from Sigma-Aldrich (St. Louis, USA). 3-(Triethoxysiyl)propylsuccinic anhydride (TEPSA, 95%) was purchased from ABCR (Karlsruhe, Germany) and 3,9-Bis(3-aminopropyl)-2,4,8,10-tetraoxaspiro [5.5] undecane (ATU) was purchased from TCY (Tokyo, Japan). All other chemicals were purchased from Panreac Química SLU (Castellar del Valles, Barcelona, Spain) inc: absolute ethanol, acetone, dimethyl

sulfoxide (DMSO), etc. All reagents were used as received without further purification. Ultrapure deionized water with resistivity of 18.2 MΩ was obtained using a Millipore Milli-Q plus system (Millipore S.A.S, Molsheim, France).

2.2 Characterization techniques

Powder X-Ray Diffraction (XRD) experiments were performed in a Philips X'Pert diffractometer equipped with Cu Kα radiation (wavelength 1.5406 Å) (Philips Electronics NV, Eindhoven, Netherlands). XRD patterns were collected in the 2ϴ range between 0.6° and 8° with a step size of 0.02° and counting time of 5 s per step. Thermogravimetric (TG measurements were performed in a Perkin Elmer Pyris Diamond TG/DTA (California, USA), with 5 ºC min^{-1} heating ramps, from room temperature (RT) to 600 ºC. Fourier transform infrared spectroscopy (FTIR) was carried out in a Nicolet (Thermo Fisher Scientific, Waltham, MA, USA) Nexus spectrometer equipped with a Goldengate attenuated total reflectance (ATR) accessory (Thermo Electron Scientific Instruments LLC, Madison, WI USA). Morphology, mesoestructural order and nanoparticles functionalization were studied by High Resolution Transmission Electron Microscopy (HRTEM) with a JEOL JEM 3000F instrument operating at 300 kV, equipped with a CCD camera (JEOL Ltd., Tokyo, Japan). Sample preparation was performed by dispersing in distilled water and subsequent deposition onto carbon-coated copper grids. A 1% PTA solution (pH 7.0) was used as staining agent in order to visualize the organic coating around MSNs.

To determine the evolution of the size and surface charge of nanoparticles by dynamic light scattering (DLS) and zeta (ζ)-potential measurements, respectively, a Zetasizer Nano ZS (Malvern Instruments, United Kingdom) equipped with a 633 nm "red" laser was used. DLS measurements were directly recorded in ethanolic colloidal suspensions. ζ-potential measurements were recorded in aqueous colloidal suspensions. For this purpose, 1 mg of nanoparticles was added to 10 mL of solvent followed by 5 min of sonication to obtain a homogeneous suspension. In both cases, measurements were recorded by placing 1 mL of suspension (0.1 mg mL^{-1}) in DTS1070 disposable folded capillary cells (Malvern Instruments). The textural properties of the materials were determined by N_2 adsorption porosimetry by using a Micromeritics ASAP 2020

(Micromeritics Co., Norcross, USA). To perform the N_2 measurements, 20-30 mg of each sample was previously degassed under vacuum for 24 h at 40 ºC temperature. The surface area (S_{BET}) was determined using the Brunauer-Emmett-Teller (BET) method and the pore volume (V_P) was estimated from the amount of N_2 adsorbed at a relative pressure around 0.97. The pore size distribution between 0.5 and 40 nm was calculated from the adsorption branch of the isotherm by means of the Barrett-Joyner-Halenda (BJH) method. The mesopore size (D_P) was determined from the maximum of the pore size distribution curve. To evaluate the different carbon environments, $^{1}H \rightarrow {}^{13}C$ CP (cross-polarization)/ MAS (magic angle spinning) solid-state nuclear magnetic resonance (NMR) measurements were performed in a Bruker AV-400-WB spectrometer (Karlsruhe, Germany) operating at 75.45 MHz. Solid samples were placed in a 4 mm zirconia rotor and spun at 12 kHz. Chemical shifts (δ) of ^{13}C were externally referred to glycine at δ = 0.0 ppm. The periods of time between successive accumulations were 3 ms and *ca* 15,000 scans were collected.

2.3 Synthesis of pure-silica MSNs (MSN)

Bare MSNs, denoted as MSN, were synthesized by the modified Stöber method using TEOS as silica source in the presence of CTAB as structure directing agent. Briefly, 1 g of CTAB, 480 mL of H_2O and 3.5 mL of NaOH (2 M) were added to a 1,000 mL round-bottom flask. The mixture was heated to 80 ºC and magnetically stirred at 600 rpm. When the reaction mixture was stabilized at 80 ºC, 5 mL of TEOS were added dropwise at 0.33 mL min^{-1} rate. The white suspension obtained was stirred during further 2 h at 80 ºC. The reaction mixture was centrifuged and washed three times with water and ethanol. Finally, the product was dried under vacuum at 40 ºC. The surfactant was removed by ionic exchange by soaking 1 g of nanoparticles in 500 mL of a NH_4NO_3 solution (10 mg mL^{-1}) in ethanol (95%) at 65 ºC overnight under magnetic stirring. The nanoparticles were collected by centrifugation (9,000 rpm, 15 min), washed twice with water and twice with ethanol and dried under vacuum at 40 ºC.

For cellular internalization studies fluorescein-labeled MSN were synthesized. For this purpose, 1 mg FITC and 2.2 µL APTES were dissolved in 100 µL ethanol and left reacting for 2 h. Then the reaction mixture was added with the 5 mL of TEOS as previously described.

2.4. Functionalization of MSN with carboxylic acid groups (MSN_{COOH})

With the aim of preferentially grafting carboxylic acid groups to the external surface of MSN, functionalization was carried out in MSN before being submitted to the surfactant extraction process [56]. Thus, 500 mg of CTAB-containing MSN were placed in a three-neck round bottom flask and dried at 80 ºC under vacuum for 24 h. Then, 125 mL of dry toluene was added and the flask was placed in an ultrasonic bath for several sonication cycles of 5 min until a good nanoparticles suspension was achieved. After that 300 µL of TEPSA were added, keeping the reaction under nitrogen atmosphere at 90 ºC for 24 h. Next, 40 mL of slightly acidified water were added in order to hydrolyze the succinic groups to carboxylic acid groups[57]. The nanoparticles were collected by centrifugation, washed three times with ethanol and dried under vacuum at 40 ºC. For deep characterization of this carboxylic acid MSNs, the surfactant removal was accomplished by solvent extraction as above mentioned, affording MSN_{COOH}.

2.5. Functionalization of MSN with a pH-cleavable linker (MSN_{ATU})

First, 300 mg of MSN_{COOH} was suspended in 50 mL PBS 1x and subjected to several sonication cycles of 5 min until a good suspension was achieved. Then, 480 mg of EDC and 180 mg of sulfo-NHS was added and stirred for 30 min. After that, the grafting of ATU to the surface of surfactant-containing MSN_{COOH} was attained by adding 2 g of ATU to the suspension and the mixture was reacted overnight. The product was filtered, washed with water and the surfactant removal was then carried out, affording MSN_{ATU}. This sample was left to dry under vacuum at 40 ºC.

2.6. Capping of MSN with PAA (MSN_{PAA})

The first step was to investigate the amount of acid-sensitive polymer that led to the most effective and uniform coating while avoiding nanoparticles aggregation. With this goal in mind 10 mg of MSN_{ATU} was suspended in 1 mL PBS (10 mM). Then 0.36, 3.6 or 36 µL PAA was added to the suspension and the resulting PAA-coated MSNs were characterized by TEM and their molecule

release performance was preliminary evaluated "in vial", as it will be described below. The most effective and most uniform coating (Fig. S1, Supporting Information) and the best preliminary release behavior (results not shown) were achieved for the lowest polymer amount, *i.e.* 0.36 µL. Thus, this amount was chosen to synthetize PAA-coated nanoparticles, named MSN_{PAA}.

2.7. ConA grafting to MSN_{PAA} (MSN_{ConA})

The covalent conjugation of ConA to MSN_{PAA} nanoparticles was acomplished using a well-known and widely reported procedure, *via* carbodiimide chemistry, whereby the amine of the protein forms and amide bond to the carboxylated nanoparticle, affording MSN_{ConA} [58,59]. For this purpose, 16 mg of MSN_{PAA} was placed in a vial and suspended in 2 mL of PBS pH 7.4 with the aid of several cycles of sonication. After that, 30 mg of EDC were added and the mixture was stirred at RT for 40 min. Then 14 mg of NHS were added and the reaction was stirred for 10 min before adding 30 mg of ConA and left to react overnight at RT. Finally, samples were filtered, washed twice with PBS pH 7.4 and dried under vacuum at 25 ºC.

2.8. Cargo loading

40 mg of MSN_{ATU} were placed in a dark glass vial and dried at 80 ºC overnight under vacuum. Then, 6 mL of $[Ru(bipy)_3]Cl_2$ (a model molecule) or DOX (an antitumor drug) aqueous solution (10 or 3 mg mL^{-1} respectively) were added and the suspension was stirred at RT. for 24 h. After that, 2.15 µL of PAA were added and stirred for 10 min before adding 96 mg of EDC and 36 mg of NHS and finally allowed to react overnight at RT. Next, samples were filtered and washed twice with PBS pH 7.4 in order to remove the $[Ru(bipy)_3]Cl_2$ or DOX adsorbed on the external surface of the nanoparticles. Finally, the products were dried under vacuum at 25 ºC. The grafting of ConA was then carried out by following the procedure previously described, leading to MSN_{ConA}@$[Ru(bipy)_3]^{2+}$ or MSN_{ConA}@DOX nanoparticles.

The amount of $[Ru(bipy)_3]^{2+}$ or DOX loaded in nanoparticles was determined from the difference between the fluorescence measurements of the initial and the recovered filtrate solutions in the step previous to ConA grafting. In both cases, two different calibration lines (one at each tested pH) were performed to eliminate the contribution of nonspecific release by pH effect.

2.9. "In vial" cargo release assays

To investigate the pH-responsive drug release performance of MSN_{ConA}, $[Ru(bipy)_3]^{2+}$ was chosen as model molecule and "in vial" time-based fluorescence release experiments in phosphate buffered saline (PBS 1x), at the two different pH values, *i.e.* 7.4 and 5.3, were carried out during 24 h. Fluorescence measurements were recorded on a PTI QuantaMaster 400 system featuring a JYF-FLUOROMAX-4 compact spectrofluorimeter single grating excitation and emission monochromator with a photomultiplier detector (PMT R928P) and an automated four-position thermostated cuvette-holder (FL-1011) (PTI, Photon Technology International, HORIBA Jobin Yvon GmbH, Germany). For temperature settings, a MTB-IFI-156-5251 refrigerated bath circulator with a peltier was used. $[Ru(bipy)_3]^{2+}$ was excited with 451 nm and showed a maximum of emission at 619 nm (excitation slit 0.38 mm, emission slit 0.38 mm, integration 0.5 s). For release experiments, the procedure reported by Bein and co-workers was used[60]. Thus, 170 µL of a 2 mg mL^{-1} nanoparticles suspension was filled into a reservoir cap sealed with a dialysis membrane (molecular weight cut-off 12,000 g mol^{-1}), which allows released dye molecules to pass into the fluorescence cuvette (that was completely filled with PBS at a given pH) while the relatively large particles are held back. Experiments were performed at a temperature of 37 ºC. On the other hand, with the aim of carrying out a more realistic experiment pH-responsive $[Ru(bipy)_3]^{2+}$ release performance of MSN_{ConA} was performed in cell culture media in order to mimic the *in vitro* conditions. These complementary experiments were performed in α-minimum essential medium (α-MEM, Sigma Chemical Company) containing 10% of heat-inactivated fetal bovine serum (FBS, Thermo Fisher Scientific) and 1% penicillin-streptomycin (BioWhittaker Europe, Verviers, Belgium) at two pH values, *i.e.* 7.4 and 5.3. The experiments were carried out at a temperature of 37 ºC during 48 h, which was the time used to accomplish *in vitro* cytotoxicity assays with cells (see Section 2.10).

2.10. Cell cultures

Cell culture tests were performed using the well-characterized mouse preosteoblastic cell line MC3T3-E1 (subclone 4, CRL-2593; ATCC, Mannassas, VA) and HOS cells derived from a

human osteosarcoma (CRL-1543; ATCC, Mannassas, VA). The tested nanoparticles were placed into each well of 6- or 24-well plates (Corning, CULTEK, Madrid, Spain) after cell seeding. MC3T3-E1 and HOS cells were then plated separately at a density of 20,000 cells cm^{-2} in 1 mL of α-minimum essential medium (MEM) or Dulbecco's modified Eagle's medium (DMEM, Sigma Chemical Company), respectively, containing 10% of FBS and 1% penicillin–streptomycin at 37 ºC in a humidified atmosphere of 5% CO_2, and incubated for different times. Some wells contained no nanoparticles as controls.

2.11. Cell viability

Cell growth was analyzed using the CellTiter 96® AQueous Assay (Promega, Madison, WI, USA), a colorimetric method for determining the number of living cells in culture. Briefly, both type of cells were cultured as described above without (control) or with the tested materials and/or different concentrations of ConA for several times. At each time, 40 µL of CellTiter 96 AQueous One Solution Reagent (containing 3-(4,5-dimethythizol-2-yl)-5-(3-carboxymethoxyphenyl)-2-(4-sul-fophe-nyl)-2H-tetrazoliumsalt (MTS) and an electron coupling reagent (phenazine ethosulfate) that allows its combination with MTS to form a stable solution was added to each well and incubated for 4 h. The absorbance at 490 nm was then measured in a Unicam UV-500 UV–visible spectrophotometer (Thermo Spectronic, Cambridge, UK).

2.12. Flow cytometry studies

MC3T3-E1 and HOS cells were cultured separately in each well of a 6-well plate. After 24h, the cells were incubated at different times in the absence or presence of the tested nanoparticles (100 µg mL^{-1}). After 2 h, cells were washed twice with PBS and incubated at 37 ºC with trypsin–EDTA solution (Sigma-Aldrich) for cell detachment. The reaction was stopped with culture medium after 5 min and cells were centrifuged at 1,000 rpm for 10 min and resuspended in fresh medium. Then, the surface fluorescence of the cells was quenched with trypan blue (0.4%) to confirm the presence of an intracellular, and therefore internalized, fluorescent signal. Flow cytometry measurements were performed at an excitation wavelength of 488 nm, green fluorescence was measured at 530 nm (FL1). The trigger was set for the green fluorescence channel (FL1). The conditions for the

data acquisition and analysis were established using negative and positive controls with the CellQuest Program of Becton–Dickinson and these conditions were maintained during all the experiments. Each experiment was carried out three times and single representative experiments are displayed. For statistical significance, at least 10,000 cells were analyzed in each sample in a FACScan machine (Becton, Dickinson and Company, USA) and the mean of the fluorescence emitted by these single cells was used.

2.13. Fluorescence microscopy

Cells were incubated with the MSNs (100 μg mL^{-1}) for 2 h. Each well was washed with cold PBS for three more times to get rid of the nanoparticles no internalized into the cells, and then fixed with 75% ethanol (kept at -20 ºC) for 10 min. After the ethanol was suck and washed three times with cold PBS, actin filaments were stained in red with Alexa Fluor® 555 Phalloidin (Thermo Fisher Scientific) for 20 mins at 1:40. The nucleus of both types of cells were stained with 4',6-diamidino-2-fenilindol (DAPI, ≥ 98%, Sigma-Aldrich) for 5 min, respectively, and then washed three times with cold PBS. Fluorescence microscopy of fluorescein-labelled MSN_{PAA} and MSN_{ConA} internalized into MC3T3-E1 and HOS cells was performed with an Evos FL Cell Imaging System (Thermo Fisher Scientific) equipped with three Led Lights Cubes (λex (nm); λem (nm)): DAPI (357/44; 447/60), GFP (470/22; 525/50), RFP (531/40; 593/40) from AMG (Advance Microscopy Group). Red channel was used to label the cytoplasm, green for nanoparticles and blue for cell nucleus.

2.14. Measurement of sialic acid levels

The contents of the resulting free N-acetylneuraminic acid were measured using a sialic acid (NANA) fluorometric assay kit (BioVision Inc., Milpitas, CA, USA) according to the manufacturer's instructions, followed by detection and analyses UV-visible. This kit utilizes an enzyme coupled reaction in which free sialic acid is oxidized resulting in development of Oxi-Red probe to give absorbance (OD = 570 nm).

2.15. Statistical analysis

Results are expressed as mean ± SEM. Statistical evaluation was carried out with nonparametric Kruskal-Wallis test and post-hoc Dunn´s test, when appropriate. A value of $p<0.05$ was considered significant.

3. Results and Discussion

3.1 Preparation and characterization of the nanosystems

Scheme 1 illustrates the different synthetic steps carried out in this work with the aim of assembling the different building blocks in to the DOX-loaded MSNs aimed at developing the final multifunctional nanodevice for antitumor therapy. It should be remarked that this is a simplified depiction that does not take into account that, during the first synthetic stages, the incorporation of organic functions takes place not only on the external surface, but also on the internal surface of the nanoparticles, as concluded after materials characterization (*vide infra*).

First, surfactant-containing MSN were reacted with TEPSA followed by succinic anhydride hydrolysis to attain carboxylic acid moieties on the MSN, affording surfactant-containing MSN_{COOH}. Then, the acid-cleavable linker (ATU) was grafted to such nanoparticles using the well-known carbodiimide chemistry and the surfactant was removed by solvent extraction, leading to MSN_{ATU} nanosystem. The next steps consisted in loading the chemotherapeutic drug DOX inside the mesoporous cavities (MSN_{ATU}@DOX) and proceed to pore capping with the polymer PAA (MSN_{PAA}@DOX) to minimize premature cargo release before reaching the acidic environment of the endo/lysosomes of the target tumor cell. Finally, ConA was covalently linked to the resulting nanosystems, providing MSN_{ConA}@DOX. The proposed pH-responsive release behavior of the full nanodevice is schematically depicted as an inset in Scheme 1. The pH-dependent stability of this acetal linker (ATU) was studied (Fig. S2), remaining stable after 24 h at pH 7.4 while breaking at acidic pH of 5.3, in good agreement with the literature [52].

With the aim of confirming the chemical grafting of the different functional groups after each step of the synthesis, all the nanosystems were deeply characterized after surfactant removal and before DOX loading, namely, MSN, MSN_{COOH}, MSN_{ATU}, MSN_{PAA} and MSN_{ConA}.

FTIR spectra evidence the successful functionalization stages of MSN, since vibration bands corresponding to the grafted chemical groups are observed (Fig. 1). FTIR spectrum of MSN displays vibration bands in the 490-1090 cm^{-1} range typical of pure silica materials. MSN_{COOH} FTIR spectrum shows an adsorption peak at 1715 cm^{-1}, owing to the C=O stretching vibration in carboxyl group[61]. A slight displacement of C=O stretching vibration (1698 cm^{-1}) and an additional absorption band located at 1636 cm^{-1} characteristic of both primary and secondary amide, provided evidence of the satisfactory grafting of ATU[62]. The polymerization is evidenced by the presence of a band at 1546 cm^{-1} characteristic of the asymmetric C-O stretching mode of pure PAA[63]. The incorporation of ConA onto the surface does not involve the addition of any new functional group but the variation in the proportion of those already present, that is the reason because new bands do not appear in the spectrum but the relative intensity of the signals is modified showing that reaction takes place.

The functionalization sequence was monitored by $^{1}H \rightarrow {}^{13}C$ CP-MAS solid-state NMR spectrum (Fig. S3, Supporting Information). Compared with pure silica MSN, where only signals corresponding to residual surfactant molecules, can be observed, MSN_{COOH} showed additional resonance signals at about 15, 19, 62 and 180 ppm, which can be assigned to characteristic carbon peaks of 1,2-bidentate carboxyl groups[61]. The appearance of two signals at 80 and 110 ppm demonstrated the presence of dioxane[64] and the presence of a well-defined signal at 175 ppm indicates that ATU was covalently attached to MSN_{COOH} by an amide bond. When the polymer is attached onto the surface the two distinct peaks of pure PAA, are observed: one appears at around 40 ppm and another at 181 ppm[65]. The former is the methine and methylene carbons, and the latter is the carboxyl carbon.

Table 1 summarizes some of the most relevant features of MSN, MSN_{PAA} and MSN_{ConA} nanosystems synthetized in this work. The differences between TGA measurements allowed determining the organic matter content incorporated in each type of nanoparticle. To determine the amount of PAA present in MSN_{PAA} sample it was necessary to measure the amount of organic matter present in the different samples before polymer incorporation (results not displayed in Table 1), *i.e.* MSN (4.5%) MSN_{COOH} (21.9%), MSN_{ATU} (28.8%) and MSN_{PAA} (36.2%), which

allowed estimating a polymer content of *ca* 7%. Finally, *ca.* 10 % was the amount of ConA existing in the final nanosystem, MSN_{ConA}.

Low-angle XRD patter of MSN display four resolved peaks that can be indexed as 10, 11, 20 and 21 reflections of a well-ordered 2D-hexagonal structure with *p6mm* plain group typical of MCM-41 (Fig. 2). Nonetheless, the intensity of such peaks XRD patters of MSN_{PAA} notably decreases, even disappearing that assigned to 21 reflection, whereas those of MSN_{ConA} exhibit a unique weak signal that can be assigned to 10 reflection.

These experimental results could be related to a loss of mesostructural order due to the PAA and ConA grafting processes in samples MSN_{PAA} and MSN_{ConA}, respectively. However, it has been widely reported that it is not easy to detect alterations in the crystal structures exclusively from powder XRD[66,67]. Actually, the disappearance of the signals in XRD patterns of coated nanosystems may be also attributed to the effective filling of the mesopore channels by PAA and ConA, as it has been previously reported for MSNs coated with gelatin and decorated in the outermost surface with folic acid as targeting ligand[31]. This fact would be in good agreement with the results derived from N_2 adsorption porosimetry discussed below, where a decrease in the textural properties of these nanosystems occurs owing to the organic matter incorporation. Moreover, this statement is in agreement with HRTEM studies of the different samples, where the preservation of the well-ordered 2D-hexagonal structure can be clearly observed, *vide infra*.

As expected, the textural parameters of nanoparticles (mainly surface area, pore volume and pore diameter), derived from N_2 adsorption porosimetry experiments, experience a significant decrease with increasing surface decoration (Table 1). N_2 adsorption-desorption isotherms are of type IV corresponding to mesoporous materials (Fig. S4, Supporting Information). The suitable treatment of the experimental data evidences a dramatically decrease in the textural properties when ranging from MSN to MSN_{PAA} and MSN_{ConA} samples, which confirms the successful incorporation of the polymer coating and the lectin to the nanoparticles. Thus, the surface area (S_{BET}) decreases from 1210 $m^2\ g^{-1}$ for MSN to 22 $m^2\ g^{-1}$ and 15 $m^2\ g^{-1}$ for MSN_{PAA} and MSN_{ConA}, respectively. The initial pore volume (V_P) of MSN decreases from 1.41 $cm^3\ g^{-1}$ to 0.11 $cm^3\ g^{-1}$ and ~ 0 $cm^3\ g^{-1}$, for MSN_{PAA} and MSN_{ConA}, respectively. Finally, the pore diameter (D_P) experiences a major decrease dropping

from 2.4 nm for MSN to a value that could not be determined in the case of MSN_{PAA} and MSN_{ConA} samples. For comparison purposes, N_2 adsorption-desorption isotherm of MSN_{ATU} sample was also registered (Fig. S4, Supporting Information), whose appropriate treatment allowed to obtain the following parameters: S_{BET} = 607 m^2 g^{-1}, V_P = 0.78 m^2 g^{-1} and D_P = 2.3 nm. These results clearly point to a decrease in the surface, pore volume and pore diameter due to the partial blocking of the mesopore entrances ascribed to ATU moieties probably grafted both in the outer and inner surface of nanoparticles. All these findings may account not only to the external polymeric covering of MSN by PAA and ConA, but also to the partial filling of the mesoporous cavities, in agreement with XRD results previously discussed.

TEM images of nanoparticles samples show a honeycomb mesoporous arrangement typical of MCM-41 (Fig. 3) Grafting of PAA and ConA does not affect the mesostructural order or MSN. The morphology of the nanoparticles is also preserved, showing spherical particles in all cases. Staining of samples with 1% PTA permitted to observe the organic matter as high contrast zones and the inorganic silica matrix as brighter areas in TEM images. The average diameter of the nanosystems estimated from the measurement of 20 nanoparticles was *ca* 160 nm, 200 and 210 nm for MSN, MSN_{PAA} and MSN_{ConA}, respectively, with a relative error of *ca.* 10%. TEM images indicate that the average thickness of the organic coating for MSN_{PAA} was *ca.* 4 nm (as indicated in Fig. 3, bottom left), whereas the appearance of small globular aggregates in MSN_{ConA} sample (yellow arrows in Fig. 3, bottom right) accounts for the presence of the protein decorating the polymeric layer.

To acquire information regarding the mean size and surface charge of the nanosystems, dynamic light scattering (DLS) and ζ-potential measurements were recorded (Fig. 3, top left). The mean hydrodynamic sizes determined by DLS were found to be 180 nm, 220 nm and 260 nm for MSN, MSN_{PAA} and MSN_{ConA}, which, as expected, are slightly higher than those estimated from TEM images. This fact is explained because DLS provides the mean diameter of nanoparticles with a solvation layer[68], whereas TEM shows the size in a dry state[69].

ζ-potential measurements in water of the different nanoparticles showed notable variations in the superficial charge (Fig. S5, Supporting Information), which are consistent with the different

functionalities incorporated in each step of the synthesis. The values change from -20.0 mV for MSN to -39.2 mV for MSN_{COOH} because of the incorporation of –COOH groups of TEPSA onto the surface of MSN. For MSN_{ATU} the ζ-potential increased to -15.0 mV what is also consistent with the incorporation of amino groups from ATU. The coating process with an acid polymer (PAA) entailed again a decrease in the ζ-potential of the so-called MSN_{PAA} until -54.4 mV (MSN_{PAA}). Finally anchoring ConA by amide linkages with the acid groups of the polymer resulted in a ζ-potential value of -34.2 mV for the entire system MSN_{ConA}. The different ζ-potencial values obtained account for the successfully PAA grafting and subsequent ConA anchorage in MSN_{PAA} and MSN_{ConA}, respectively.

3.2. "In vial" cargo release experiments

$[Ru(bipy)_3]^{2+}$ was used as model molecule to evaluate the pH-responsiveness of the final nanosystem, MSN_{ConA}. As indicated in the experimental section, the cargo loading was carried out by dispersing 40 mg of MSN_{ATU} nanoparticles into a concentrated solution of $[Ru(bipy)_3]Cl_2$ (10 mg mL^{-1}) and stirred at RT for 24 h. Then PAA capping was performed in situ via EDC-NHS chemistry. After washing and isolation of molecule-loaded MSN_{PAA} samples, ConA was covalently grafted (for further details see experimental section). The estimated amount of $[Ru(bipy)_3]^{2+}$ loaded into the nanosystems was found to be 5.9% in weight. In the case of DOX, the amount of drug incorporated into the nanoparticles was 6.9% in weight. The decrease in the V_P derived from N_2 adsorption measurements (results not shown) confirms the incorporation of the cargoes into the mesoporous channels. The pH-responsive drug delivery behavior of the final nanosystem, MSN_{ConA}, under physiological relevant conditions mimicking extracellular environment (pH 7.4) and those of endosomes or lysosomes (pH ≤ 5.5) $[Ru(bipy)_3]^{2+}$ was evaluated "in vial" in two different media: phosphate buffered saline (PBS) and cell culture medium. Fig. 4.A shows the cargo release profiles from MSN_{ConA} after soaking in a buffered solution (PBS 1x) at pH 7.4 and pH 5.3 during 24 h and monitored by fluorescence excitation spectroscopy under continuous settings. Release profiles can be adjusted to first-order kinetic model by introducing an empirical non-ideality factor (δ) to give the following equation (Eq. 1) [70]:

$$Y = A\,(1-e^{-kt})^{\delta} \qquad \text{(Eq. 1)}$$

being *Y* the percentage of $[Ru(bipy)_3]^{2+}$ released at time t, *A* the maximum amount of $[Ru(bipy)_3]^{2+}$ released (in percentage), and *k* the release rate constant. The values for δ are comprised between 1 for materials that obeys first-order kinetics, and 0, for materials that release the loaded cargo in the very initial time of test. The parameters of the kinetic fitting shown in Fig. 4.A ($R^2 > 0.99$) indicate that, whereas the maximum amount of $[Ru(bipy)_3]^{2+}$ released is *ca.* 71% of the total loaded molecule at pH = 5.3 after 24 h of assay, a notable amount of the cargo is retained at pH 7.4. At the two pH values tested, the obtained δ values are very similar, in the 0.7–0.8 range, pointing to a near first order kinetics with a slight contribution of an initial burst release of the loaded molecules. Nonetheless, at pH 5.3 the total molecule release is almost 3-fold higher than that at pH 7.4, which is associated to a *k* value twice greater under acidic conditions. The two modal release curves owing to the two different slopes obtained in the same delivery curve at both pH values could be explained by taking into account that the characterization of the different materials points to the functionalization not only of the external but also of the porous internal structure of MSN. Thus, the $[Ru(bipy)_3]^{2+}$ release mechanism would be a combination of simple diffusion of molecules not being affected by the presence of the ATU linker, with acid-triggered linkage delivery.

With the aim of getting information about cargo release performance of MSN_{ConA} nanosystem under more realistic conditions mimicking the *in vitro* conditions, additional "in vial" $[Ru(bipy)_3]^{2+}$ release assays in cell culture media were carried out. These complementary experiments were performed in α-MEM containing 10% of heat-inactivated FBS and 1% penicillin-streptomycin at two pH values, *i.e.* 7.4 and 5.3, as described in the experimental section. The amount of molecule released to the complemented culture media was monitored during 48 h of assay, which was the time used for the *in vitro* cytotoxicity studies with DOX-loaded nanoparticles. The results are displayed in Fig. 4.B. In this case, the molecule release profiles at both pH values are totally different to those obtained in PBS, and they can be properly adjusted to zero-order or linear kinetics ($R^2 > 0.99$) according to Eq. 2:

$$Y = B + kt \qquad \text{(Eq. 2)}$$

being *Y* the percentage of $[Ru(bipy)_3]^{2+}$ released at time t, *B* the amount of $[Ru(bipy)_3]^{2+}$ released (in percentage) at t = 0, and *k* the release rate constant. The parameters of the kinetic fitting displayed in Fig. 4.B indicate that the amount of molecule release at t = 0 is almost depreciable at both pH values. After 48 h of assay only *ca.* 5% of molecule is released from MSN_{ConA} at pH 7.4, whereas almost 30% of the entrapped Ru(II) complex is released at pH 5.3, *i.e.* the amount of released cargo is 6-fold higher under acidic conditions than at physiological pH. This fact agrees with the release rate constant, which is 5 times faster at pH 5.3 than at pH 7.4, with values of 0.555 h^{-1} and 0.112 h^{-1}, respectively.

When comparing the results obtained in protein-free PBS media (Fig. 4.A) with those in protein-containing media (Fig. 4.B), the more remarkable aspects concern both the modification in the molecule release profiles and the maximum amount of released cargo. The results obtained in complemented α-MEM point to the coverage of the nanoparticles by a series of proteins from 10% FBS through a process called "protein corona effect"[71]. The formation of a "protein corona" onto the surface of the nanoparticles can shield the nanocarriers, thus partially blocking the mesopore entrances and, consequently, altering the cargo release profiles [72]. Herein, the protein corona would be significantly reducing the burst effect and provoking a more-sustained release of the entrapped $[Ru(bipy)_3]^{2+}$ than in protein-free PBS media.

3.2. *In vitro* biological evaluation

Once MSN_{ConA} sample was deeply characterized and its pH-sensitive drug release capability was proved "in vial", we proceeded to investigate its *in vitro* performance as selective drug delivery nanocarrier. To evaluate the *in vitro* biological behavior of our nanosystem and its potential application in bone cancer treatment, nanoparticles were incubated in the presence of two types of bone cells populations: MC3T3-E1 preosteoblastic cell line, and HOS human osteosarcoma cells.

Herein, the grafting of ConA to the outermost surface of our nanosystems aims at playing a key role, acting as targeting ligand that permits the selective internalization of the nanocarrier by bone cancer cells and not by healthy ones. Once there, the acidic environment of the endo/lysosomes cellular compartments would trigger the release of the cytotoxic cargo.

The first step consisted in evaluating the capability of ConA-conjugated (MSN_{ConA}) and ConA-free (MSN_{PAA}) nanoparticles to be internalized by MC3T3-E1 and HOS cells. To attain this goal, both types of nanoparticles were labelled with fluorescein, as previously described in the experimental section. Cellular uptake and internalization of fluorescein-labelled MSN_{ConA} and MSN_{PAA} nanoparticles were investigated by flow cytometry and fluorescence microscopy in MC3T3-E1 and HOS cells in contact with (100 µg mL^{-1}) for 2 h (Fig. 5). After 2 h of cell culture, MSN_{ConA} internalization and fluorescence intensity in HOS cells significantly increase compared to MSN_{PAA}, and they are always higher than those in MC3T3-E1 cells.

The cellular uptake results obtained by flow cytometry were also confirmed by fluorescence microscopy using fluorescein-labelled nanoparticles after 2 h (representative images in Fig. 6). The highest amount of internalized nanoparticles corresponds to MSN_{ConA} ones after being in contact with HOS osteosarcoma cells. Notice that, in this case, there is a perceptible variation in the morphology and disposition of actin filaments, which make us hypothesizing that those cells may be in a preapoptotic state (Fig. 6). This finding could be attributed to some cellular damage that ConA may be exerting in HOS cells (see Fig. S6, Supporting Information), as reported in the literature for various cancer cell lines[73-75]. Nonetheless, no significant cell viability decrease has been observed during cytotoxicity assays by MTS for MSN_{ConA} concentrations up to 144 µg mL^{-1} (Fig. S7, Supporting Information).

The next step was to investigate the ligand-receptor interactions that would be promoting preferential MSN_{ConA} internalization into HOS cancer cells. In this context, in recent years, sialic acids, a type of glycans attached to glycoproteins on the cell, have been studied as disease-associated carbohydrate derivatives, because their expression provides many opportunities for the appraisal of the cell processes[76,77]. For instance, Cho *et al.* designed lectin-tagged fluorescent polymeric nanoparticles as potential bioimaging probes for detecting diseased cells by the union lectin-sialic acids[78]. Through cellular experiments, they successfully detected sialic acid overexpression on cancerous cells with high specificity.

Thus, to confirm the possible overexpression of sialic acid in HOS cells compared with MC3T3-E1 cells, and their interaction with ConA, we measured the N-acetylneuraminic acid levels. This

acid is the most common member of sialic acid derivatives and is found widely distributed in animal tissues. We found that N-acetylneuraminic acid levels in HOS cells were significantly higher than in MC3T3-E1 cells: 600 ± 1 nmol μg^{-1} protein in HOS cells vs. 100 ± 2 nmol μg^{-1} protein in MC3T3-E1 cells. These results suggest that the presence of ConA in the surface of the nanoparticles allows the binding with sialic acid and improving the selective internalization of MSN_{ConA} in HOS cells where the sialic acid levels were 6-fold increased. It is true that MSN_{ConA} can be uptaken by non-tumor MC3T3-E1 cells that are non-overexpressing sialic acid, but this internalization rate was always higher in HOS cells. Therefore, our group and others have previously demonstrated that MC3T3-E1 cells internalized itself different types of nanoparticles [30,31,36,79,80] Moreover, probably this N-acetylneuraminic acid levels overexpression is not the only mechanism implicated in the high rate of MSNConA internalization. Further studies are needed to confirm these hypotheses.

Once demonstrated the capability of MSN_{ConA} nanoparticles to be preferentially internalized by HOS cells than by MC3T3-E1 cells, the next goal was to investigate and compare the in vitro performance of DOX-loaded lectin-conjugated (MSN_{ConA}@DOX) and lectin-free (MSN_{PAA}@DOX) nanosystems in cultures of both cell types at different nanoparticles concentrations. However, evaluating the killing capability of free DOX towards both cell types is necessary to compare the efficiency and selectivity of the here developed nanotransporter. Thus, different amounts of free DOX (0, 2.5, 5, 10 and 20 $\mu g\ mL^{-1}$) were used, and the results indicate that cell death induced by DOX is very high and shows a linear dose-dependent concentration both in preosteoblastic MC3T3-E1 and osteosarcoma HOS cells (Fig. S8, Supporting Information). This accounts for the high and unselective cytotoxicity of this drug.

Then, we performed and *in vitro* cytotoxicity study (by a MTS assay) with DOX concentrations (2.5 and 10 $\mu g\ mL^{-1}$) incorporated in MSN_{ConA} and MSN_{PAA} nanoparticles in the presence of MC3T3-E1 or HOS cells at 48 h (Fig. 7). Comparing the toxicity of MSN_{ConA}@DOX vs. that of MSN_{PAA}@DOX, it is observed that MSN_{ConA}@DOX causes increased cell death than MSN_{PAA}@DOX, and that this increase is much more significant in HOS cells that in MC3T3-E1. Actually, it should be highlighted that this effect is much more obvious at very low DOX

concentrations (2.5 μg mL^{-1}). Thus, after 48 h of assay MC3T3-E1 cells does not experience any cytotoxic effect after being incubated with 2.5 μg mL^{-1} of DOX loaded in both nanosystems. Oppositely, HOS cells viability decreases to *ca.* 40% after exposition to 2.5 μg mL^{-1} of drug loaded into MSN_{PAA}. This value is quite similar to that for HOS cells after exposure to free DOX (Fig. S8, Supporting Information). Nonetheless, the antitumor effect of MSN_{ConA} towards HOS cells increases 8-fold compared to MSN_{PAA} (Fig. S8, Supporting Information).

4. Conclusions

In this work we have developed a multifunctional nanodevice featuring selectivity towards human osteosarcoma cells and pH-responsive antitumor drug delivery capability. The synergistic combination of both properties into a unique nanosystem produces an amplification of the antitumor efficacy.

This innovative nanodevice is based in DOX-loaded MSNs nanoplatforms where different building blocks are assembled: i) a PAA polymeric shell, anchored *via* an acid cleavable linker, to prevent premature cargo release and provide the nanosystem of pH-responsive capability; ii) a targeting ligand consisting in the lectin ConA grafted to PAA, to increase the selectivity towards cancer cells whereas significantly preserving the viability of healthy cells.

In vitro assays reveal that the internalization degree of lectin-conjugated nanosystems into human osteosarcoma cells is 2 times higher than in human preosteoblastic cells. Moreover, only very small DOX concentrations (2.5 μg mL^{-1}) are needed to attain *ca* 100% antitumor efficacy against osteosarcoma cells compared to healthy bone cells, whose viability is preserved. Moreover, the antitumor effect is increased up to 8-fold compared to that caused by the free drug.

These outcomes prove that the synergistic assembly of different building blocks into a unique nanoplatform increases antitumor effectiveness and decreases toxicity towards healthy cells, which constitutes a new paradigm in targeted bone cancer therapy.

Apendix A. Supplementary data

Supplementary data associated with this article can be found in the online version.

Acknowledgements

MVR acknowledges funding from the European Research Council (Advanced Grant VERDI; ERC-2015-AdG Proposal No. 694160). The authors also thank to Spanish Ministerio de Economía y Competitividad (MINECO) (Project MAT2015-64831-R). The XRD measurements, $^{1}H \rightarrow {}^{13}C$ solid-state NMR spectra and internalization studies were performed at C.A.I. Difracción de Rayos X, C.A.I. Resonancia Magnética Nuclear and C.A.I. Citometría de Flujo from UCM (Spain), respectively. TEM studies were performed at ICTS National Centre for Electron Microscopy (Spain).

References

[1] K.D. Miller, R.L. Sigel, C.C. Lin, A.B. Mariotto, J.L. Kramer, J.H. Rowland, K.D. Stein, R. Alteri, A. Jemal, Cancer treatment and survivorship statistics, CA Cancer J. Clin. 66 (2016) 271–289.

[2] O.C. Farokhzad, R. Langer, Impact of nanotechnology on drug delivery, ACS Nano 3 (2009) 16–20.

[3] D. Peer, J.M. Karp, S. Hong, O.C. Farokhzad, R. Margalit, R. Langer, Nanocarriers as an emerging platform for cancer therapy, Nature Nanotechnol. 2 (2007) 751–760.

[4] S. Mura, J. Nicolas, P. Couvreur, Stimuli-responsive nanocarriers for drug delivery, Nature Mater. 12 (2013) 991–1003.

[5] G.S.R. Raju, L. Benton, E. Pavitra, J.S. Yu, Multifunctional nanoparticles: recent progress in cancer therapeutics, Chem. Commun. 51 (2015) 13248–13259.

[6] W.Q. Lim, S.Z.F. Phua, H.V. Xu, S. Sreejith, Y. Zhao, Recent advances in multifunctional Silica-based hybrid nanocarriers for bioimaging and cancer therapy, Nanoscale 8 (2016) 12510–12519.

[7] M. Karimi, A. Ghasemi, P.S. Zangabad, R. Rahighi, S.M.M. Basri, H. Mirshekari, M. Amiri, Z.S. Pishabad, A. Aslani, M. Bozorgomid, D. Ghosh, A. Beyzavi, A. Vaseghi, A.R. Aref, L. Haghani, S. Bahramia, M.R. Hamblin, Smart micro/nanoparticles in stimulus-responsive drug/gene delivery systems, Chem. Soc. Rev. 45 (2016) 1457–1501.

[8] M. Vallet-Regí, F, Balas, D. Arcos, Mesoporous materials for drug delivery, Angew. Chem. Int. Ed. 46 (2007) 7548–7558.

[9] Z. Li, J.C. Barnes, A. Bosoy, J.F. Stoddart, J.I. Zink, Mesoporous silica nanoparticles in biomedical applications, Chem. Soc. Rev. 41 (2012) 2590–2605.

[10] J.L. Vivero-Escoto, I.I. Slowing, B.G. Trewyn, V.S.-Y. Lin, Mesoporous silica nanoparticles for intracellular controlled drug delivery, Small 6 (2010) 1952–1967.

[11] A. Popat, S.B. Hartono, F. Stahr, J. Liu, S.Z. Qiao, G.Q.M. Lu, Mesoporous silica nanoparticles for bioadsorption, enzyme immobilisation, and delivery carriers, Nanoscale 3 (2011) 2801–2818.

[12] F. Tang, L. Li, D. Chen, Mesoporous silica nanoparticles: Synthesis, biocompatibility and drug delivery, Adv. Mater. 24 (2012) 1504–1534.

[13] P. Yang, S. Gai, J. Lin, Functionalized mesoporous silica materials for controlled drug delivery, Chem. Soc. Rev. 41 (2012) 3679–3698.

[14] Y. Chen, H. Chen, J. Shi, In vivo bio-safety evaluations and diagnostic/therapeutic applications of chemically designed mesoporous silica nanoparticles, Adv. Mater. 25 (2013) 3144–3476.

[15] C. Argyo, V. Weiss, C. Bräuchle, T. Bein, Multifunctional mesoporous silica nanoparticles as a universal platform for drug delivery, Chem. Mater. 26 (2014) 435–451.

[16] M. Martínez-Carmona, M. Colilla, M. Vallet-Regí, Smart mesoporous nanomaterials for antitumor therapy, Nanomaterials 5 (2015) 1906–1937.

[17] A. Baeza, M. Colilla, M.Vallet-Regí, Advances in mesoporous silica nanoparticles for targeted stimuli-responsive drug delivery, Expert. Opin. Drug Deliv. 12 (2015) 319–337.

[18] J.L. Paris, P. de la Torre, M. Manzano, M.V. Cabañas, A.I. Flores, M. Vallet-Regí, Decidua-derived mesenchymal stem cells as carriers of mesoporous silica nanoparticles. *In vitro* and *in vivo* evaluation on mammary tumors, Acta Biomater. 33 (2016) 275–282.

[19] R.R. Castillo, M. Colilla, M. Vallet-Regí, Advances in mesoporous silica-based nanocarriers for co-delivery and combination therapy against cancer, Expert Opin. Drug Deliv. 14 (2017) 229–243.

[20] J. Lu, M. Liong, V. Li, J.I. Zink, F. Tamanoi, Biocompatibility, biodistribution, and drug-delivery efficiency of mesoporous silica nanoparticles for cancer therapy in animals, Small 6 (2010) 1794–1805.

[21] Y. Zhao, X. Sun, G. Zhang, B.G. Trewyn, I.I. Slowing, V.S. Lin, Interaction of mesoporous silica nanoparticles with human red blood cell membranes: size and surface effects, ACS Nano 5 (2011) 1366–1375.

[22] J.L. Paris, M.V. Cabañas, M. Manzano, M. Vallet-Regí, Polymer-grafted mesoporous silica nanoparticles as ultrasound-responsive drug carriers, ACS Nano 9 (2015) 11023–11033.

[23] M. Martínez-Carmona, A. Baeza, M.A. Rodríguez-Milla, J. García-Castro, M. Vallet-Regí, Mesoporous silica nanoparticles grafted with a light-responsive protein shell for highly cytotoxic antitumoral therapy, J. Mater. Chem. B 3 (2015) 5746–5752.

[24] E. Guisasola, A. Baeza, M. Talelli, D. Arcos, M. Moros, J.M. de la Fuente, M. Vallet-Regí, Magnetic-responsive release controlled by hot spot effect, Langmuir 31 (2015) 12777–12782.

[25] P. Saint-Cricq, S. Deshayes, J.I. Zink, A.M. Kasko, Magnetic field activated drug delivery using thermodegradable azo-functionalised PEG-coated core–shell mesoporous silica nanoparticles, Nanoscale 7 (2015) 13168–13172.

[26] Q. Lei, W.-X. Qiu, J.-J. Hu, P.-X. Cao, C.-H. Zhu, H. Cheng, X.-Z. Zhang, Multifunctional mesoporous silica nanoparticles with thermal-responsive gatekeeper for NIR light-triggered chemo/photothermal-therapy, Small 12 (2016) 4286–4298.

[27] X. Li, W. Zhao, X. Liu, K. Chen, S. Zhu, P. Shi, Y. Chen, J. Shi, Mesoporous manganese silicate coated silica nanoparticles as multi-stimuli-responsive T1-MRI contrast agents and drug delivery carriers, Acta Biomater. 30 (2016) 378–387.

[28] S. Chai, Y. Guo, Z. Zhang, Z. Chai, Y. Ma and L. Qi, Cyclodextrin-gated mesoporous silica nanoparticles as drug carriers for red light-induced drug release, Nanotechnology 28 (2017) 145101.

[29] J.L. Paris, P. de la Torre, M.V. Cabañas, M. Manzano, M. Grau, A.I. Flores, M.Vallet-Regí, Vectorization of ultrasound-responsive nanoparticles in placental mesenchymal stem cells for cancer therapy, Nanoscale, 9 (2017) 5528–5553.

[30] M. Martínez-Carmona, D. Lozano, A. Baeza, M. Colilla, M. Vallet-Regí. A novel visible light responsive nanosystem for cancer treatment, Nanoscale (2017) doi: 10.1039/C7NR05050J.

[31] M. Martínez-Carmona, D. Lozano, M. Colilla, M. Vallet-Regí, Selective topotecan delivery to cancer cells by targeted pH-sensitive mesoporous silica nanoparticles, RSC Adv. 6 (2016) 50923–50932.

[32] Z. Wang and L. Gan, Using hyaluronic acid-functionalized pH stimuli-responsive mesoporous silica nanoparticles for targeted delivery to CD44-overexpressing cancer cells, Int. J. Nanomedicine 11 (2016) 6485–6497.

[33] A. Kienzle, S. Kurch, J. Schlöder, C. Berges, R. Ose, J. Schupp, A. Tuettenberg, H. Weiss, J. Schultze, S. Winzen, M. Schinnerer, K. Koynov, M. Mezger, N. K. Haass, W. Tremel, H. Jonuleit, Dendritic mesoporous silica nanoparticles for pH-stimuli-responsive drug delivery of TNF-alpha, Adv. Healthc. Mater. 6 (2017) 1700012.

[34] S. Zhao, M. Xu, C. Cao, Q. Yu, Y. Zhou, J. Liu, A redox-responsive strategy using mesoporous silica nanoparticles for co-delivery of siRNA and doxorubicin, J. Mater. Chem. B, 5 (2017) 6908–6919.

[35] X. Chen, H. Sun, J. Hu, X. Han, H. Liu, Y. Hu, Transferrin gated mesoporous silica nanoparticles for redox-responsive and targeted drug delivery, Colloids Surf. B Biointerfaces, 152 (2017) 77–84.

[36] M. Gisbert-Garzarán, D. Lozano, M. Vallet-Regí, M. Manzano, Self-immolative polymers as novel pH-responsive gate keepers for drug delivery, RSC Adv. 7 (2017) 132–136.

[37] J. Wen, K. Yang, Y. Xu, H. Li, F. Liu, S. Sun, Construction of a triple-stimuli-responsive system based on cerium oxide coated mesoporous silica nanoparticles, Sci. Rep. 6 (2016) article number: 38931, DOI:10.1038/srep38931.

[38] Y. Tian, R. Guo, Y. Jiao, Y. Sun, S. Shen, Y. Wang, D. Lu, X. Jiang, W. Yang, Redox stimuli-responsive hollow mesoporous silica nanocarriers for targeted drug delivery in cancer therapy, Nanoscale Horiz. 1 (2016) 480–487.

[39] D. Xiao, H.-Z Jia, J. Zhang, C.–W. Liu, R.–X. Zho, X.–Z. Zhang, A dual-responsive mesoporous silica nanoparticle for tumor-triggered targeting drug delivery, Small 10 (2014) 591–598.

[40] Q. Zhao, J. Liu, W. Zhu, C. Sun, D. Di, Y. Zhang, P. Wang, Z. Wang, S. Wang, Dual-stimuli responsive hyaluronic acid-conjugated mesoporous silica for targeted delivery to CD44-overexpressing cancer cells, Acta Biomater. 23 (2015) 147–156.

[41] X. Chen, Z. Liu, Dual responsive mesoporous silica nanoparticles for targeted co-delivery of hydrophobic and hydrophilic anticancer drugs to tumor cells, J. Mater. Chem. B 4 (2016) 4382–4388.

[42] M.P. Alvarez-Berríos, J. L. Vivero-Escoto, *In vitro* evaluation of folic acid-conjugated redox-responsive mesoporous silica nanoparticles for the delivery of cisplatin, Int. J. Nanomed. 11 (2016) 6251–6265.

[43] H. Ganjavi, M. Gee, A. Narendran, N. Parkinson, M. Krishnamoorthy, M. Freedman, D. Malkin, Adenovirus-mediated p53 gene therapy in osteosarcoma cell lines: sensitization to cisplatin and doxorubicin, Cancer Gene Ther. 13 (2006) 415–419.

[44] I. Müller, A. Jenner, G. Bruchelt, D. Niethammer, B. Halliwell, Effect of concentration on the cytotoxic mechanism of doxorubicin–apoptosis and oxidative DNA damage, Biochem. Biophys. Res. Commun. 230 (1997) 254–257.

[45] C.-H. Lee, S.–H. Cheng, I.-P. Huang, J.S. Souris, C.-S. Yang, C.-Y. Mou, L.-W. Lo, Intracellular pH-Responsive mesoporous silica nanoparticles for the controlled release of anticancer chemotherapeutics, Angew. Chem. Int. Ed. 49 (2010) 8214–8219.

[46] Q. Qu, X. Ma, Y, Zhao, Targeted delivery of doxorubicin to mitochondria using mesoporous silica nanoparticle nanocarriers, Nanoscale, 7 (2015) 16677–16686.

[47] L. Yuan, Q. Tang, D. Yang, J.Z. Zhang, F. Zhang, J. Hu, Preparation of pH-responsive mesoporous silica nanoparticles and their application in controlled drug delivery, J. Phys. Chem. C 115 (2011) 9926–9932.

[48] S. Shahabi, S. Döscher, T. Bollhorst, L. Treccani, M. Maas, R. Dringen, K. Rezwan, Enhancing cellular uptake and doxorubicin delivery of mesoporous, silica nanoparticles via surface functionalization: effects of serum, ACS Appl. Mater. Interfaces 7 (2015) 26880–26891.

[49] S. Khatoon, H.S. Han, M. Lee, H. Lee, D.-W. Jung, T. Thambi, M. Ikram, Y.M. Kang, G.-R. Yi, J. H. Park, Zwitterionic mesoporous nanoparticles with a bioresponsive gatekeeper for cancer therapy, Acta Biomater. 40 (2016) 282–292.

[50] W. Sun, Y. Han, Z. Li, K. Ge, J. Zhang, Bone-targeted mesoporous silica nanocarrier anchored by zoledronate for cancer bone metastasis, Langmuir 32 (2016) 9237–9244.

[51] R.C.H. Wong, D.K.P. Ng, W.-P. Fong, P.-C. Lo, Encapsulating pH-responsive doxorubicin–phthalocyanine conjugates in mesoporous silica nanoparticles for combined photodynamic therapy and controlled chemotherapy, Chem. Eur. J. (2017), DOI: 10.1002/chem.201703188.

[52] R. Liu, Y. Zhang, X. Zhao, A. Agarwal, L. J. Mueller, P. Feng, pH-responsive nanogated ensemble based on gold-capped mesoporous silica through an acid-labile acetal linker, J. Am. Chem. Soc. 132 (2010) 1500–1501.

[53] M. Chen, X. He, K. Wang, D. He, S. Yang, P. Qiu, S. Chen, A pH-responsive polymer/mesoporous silica nano-container linked through an acid cleavable linker for intracellular controlled release and tumor therapy in vivo, J. Mater. Chem. B 2 (2014) 428–436.

[54] D.H. Dube, C.R. Bertozzi, Glycans in cancer and inflammation-potential for therapeutics and diagnostics, Nature Rev. Drug Discov. 4 (2005) 477–488.

[55] E.J.M. Van Damme, W.J. Peumans, A. Barre, P. Rougé, Plant lectins: A composite of several distinct families of structurally and evolutionary related proteins with diverse biological roles, Crit. Rev. Plant Sci. 17 (2010) 575–692.

[56] F. de Juan, E. Ruiz-Hitzky, “Selective functionalization of Mesoporous Silica”, Adv. Mater. 12 (2000) 430-432.

[57] C. Schramm, B. Rinderer, Investigation of the hydrolysis of (3-triethoxysilylpropyl) succinic acid anhydride by means of FT-IR, J. Mater. Sci. 43 (2008) 4215–4219.

[58] R.A. Sperling, W.J. Parak, Surface modification, functionalization and bioconjugation of colloidal inorganic nanoparticles, Phil. Trans. R. Soc. A 368 (2010) 1333–1383.

[59] E. Mahon, A. Salvati, F.B. Bombelli, I. Lynch, K.A. Dawson, Designing the nanoparticle-biomolecule interface for "targeting and therapeutic delivery", J. Control. Release 161 (2012) 164-174.

[60] A. Schlossbauer, J. Kecht, T. Bein, Biotin-avidin as a protease-responsive cap system for controlled guest release from colloidal mesoporous silica, Angew. Chem. Int. Ed. 48 (2009) 3092–3095.

[61] H. He, H. Xiao, H. Kuang, Z. Xie, X. Chen, X. Jing, Y. Huang, Synthesis of mesoporous silica nanoparticle-oxaliplatin conjugates for improved anticancer drug delivery, Colloid. Surf. B. 117 (2014) 75–81.

[62] L. J. Bellamy, Advances in infrared group frequencies, Chapman and Hall Ltd., third edition, New York, U.S.A, 1975.

[63] Q. Ju, W. Luo, Y. Liu, H. Zhu, R. Li, X, Chen. Poly (acrylic acid)-capped lanthanide-doped BaFCl nanocrystals: synthesis and optical properties, Nanoscale 2 (2010) 1208–1212.

[64] T. Chen, H. Yu, N. Yang, M. Wang, C. Ding, J. Fu, Graphene quantum dot-capped mesoporous silica nanoparticles through an acid-cleavable acetal bond for intracellular drug delivery and imaging, J. Mater. Chem. B 2 (2014) 4979–4982.

[65] T. Miyoshi, K. Takegoshi, K. Hikichi, High-Resolution Solid State ^{13}C N.M.R, Study of the interpolymer interaction, morphology and chain dynamics of the poly(acrylic acid)/poly(ethylene oxide), Complex. Polymer 38 (1997) 2315–2320.

[66] O. Terasaki, T. Ohsuna, Z. Liu, Y. Sakamoto, A.E. García-Bennet, Structural study of mesoporous materials by electron microscopy, Stud. Surf. Sci. Catal. 148 (2004) 261–288.

[67] M. Martínez-Carmona, M. Colilla, M.L. Ruiz-González, J.M. González-Calbet, M. Vallet-Regí, M. High resolution transmission electron microscopy: A key tool to understand drug release from mesoporous matrices, Microporous Mesoporous Mater. 225 (2016) 399–410.

[68] J. Ge, Y. Yin, Magnetically tunable colloidal photonic structures in alkanol solutions. Adv. Mater. 20 (2008) 3485–3491.

[69] T. Ito, L. Sun, M.A. Bevan, R.M. Crooks, Comparison of nanoparticle size and electrophoretic mobility measurements using a carbon-nanotube-based coulter counter, dynamic

light scattering, transmission electron microscopy, and phase analysis light scattering, Langmuir 20 (2004) 6940–6945.

[70] F. Balas, M. Manzano, M. Colilla, M. Vallet-Regi, L-Trp adsorption into silica mesoporous materials to promote bone formation, Acta Biomater. 4 (2008) 514–522.

[71] M. Mahmoudi, I. Lynch, M.R. Ejtehadi, M.P. Monopoli, F.B. Bombelli, S.Laurent, Protein−nanoparticle interactions: opportunities and challenges, Chem. Rev. 111 (2011) 5610–5637.

[72] S. Behzadia, V. Serpooshan, R. Sakhtianchic, B. Müller, K. Landfester, D. Crespy, M. Mahmoudi, Colloids Surf. B Biointerfaces 123 (2014) 143–149.

[73] C.–P. Chang, M.–C. Yang, H.–S. Liu, Y.–S. Lin, H.–Y. Lei, Concanavalin A induces autophagy in hepatoma cells and has a therapeutic effect in a murine in situ hepatoma model, Hepatology 45 (2007) 286–296.

[74] W.–W. Li, J.–Y. Yu, H.–L. Xu, J.–K. Bao, Concanavalin A: A potential anti-neoplastic agent targeting apoptosis, autophagy and anti-angiogenesis for cancer therapeutics. Biochem. Biophys, Res. Commun. 414 (2011) 282–286.

[75] Z. Shi, J. Chen, C. Li. C, N. An, Z.J. Wang, S.L. Yang, K.F. Huang, J.K. Bao, Antitumor effects of Concanavalin A and sophora flavescens lectin *in vitro* and *in vivo*, Acta Pharmacol. Sin. 35 (2014) 248–256.

[76] Y. Kaneko, F. Nimmerjahn, J.V. Ravetch, Anti-inflammatory activity of immunoglobulin G resulting from Fc sialylation, Science 313 (2006) 670–673.

[77] O.M.T. Pearce, H. Läubli, Sialic acids in cancer biology and immunity, Glycobiol. 26 (2016) 111–128.

[78] J. Cho, K. Kushiro, Y. Teramura, M. Takai, Lectin-tagged fluorescent polymeric nanoparticles for targeting of sialic acid on living cells, Biomacromolecules 15 (2014) 2012–2018.

[79] B. Baumann, R. Wittig, Mika Lindén, Mesoporous silica nanoparticles in injectable hydrogels: factors influencing cellular uptake and viability, Nanoscale 9 (2017) 12379-12390.

[80] V. López, M.R. Villegas, V. Rodríguez, G. Villaverde, D. Lozano, A. Baeza, M. Vallet-Regí, ACS Appl. Mater. Interfaces 9 (2017) 26697-26706.

Figure captions

Scheme 1. Schematic illustration of the synthetic steps involved in the formation of tumor-targeted DOX-loaded nanosystem (MSN_{ConA}@DOX) consisting of MSNs encapsulating DOX, grafted with a pH-cleavable linker (ATU), coated with an acid-degradable polymer (PAA) and covalently linked to the lectin ConA to obtain the final nanodevice. The pH-responsive behavior of the nanocarrier is depicted as an inset.

Fig. 1. FTIR spectra of the different nanosystems synthetized in this work.

Fig. 2. Low-angle XRD patterns of the different nanosystems synthetized in this work.

Fig. 3. Hydrodynamic size, measured by DLS, and TEM images of the different nanosystems synthetized in this work. To carry out TEM studies samples were stained with 1% of phosphotungstic acid (PTA).

Fig. 4. "In vial" release profiles of $[Ru(bipy)_3]^{2+}$ model molecule from MSN_{ConA} nanodevices when soaked in: A) phosphate saline solution (PBS) at pH 7.4 and 5.3 for 24 h; and B) α-MEM containing 10% of heat-inactivated FBS and 1% penicillin-streptomycin at pH 7.4 and 5.3 for 48 h.

Fig. 5. Cellular uptake (A) and fluorescence intensity (B) of fluorescein-labeled MSN_{PAA} and MSN_{ConA} nanosystems measured by flow cytometry at 2 h of cell culture of MC3T3-E1 and HOS cells. Representative flow cytometry images are shown (A). Data are mean ± SEM of 3 independent experiments performed at least in triplicate *$p < 0.05$ vs. corresponding control without nanoparticles; **$p < 0.05$ vs. corresponding control with nanoparticles; #$p < 0.05$ vs. corresponding and same condition in MC3T3-E1 cells.

Fig. 6. Representative fluorescence microscopy images of MC3T3-E1 and HOS cells incubated with fluorescein-labeled MSN_{PAA} and MSN_{ConA} nanosystems at 2 h of cell culture. Blue fluorescence (nuclei), red (actin filaments), green fluorescence (fluorescein labeled nanoparticles).

Fig. 7. Cytotoxicity assay measured by MTS reduction in MC3T3-E1 and HOS cells with different concentrations (2.5 and 10 µg mL^{-1}) of DOX-loaded MSN_{PAA} and MSN_{ConA} nanosystems at 48 h of cell culture. Data are mean ± SEM of 3 independent experiments performed at least in triplicate. #$p < 0.05$ vs. 2.5 µg/mL corresponding DOX-loaded nanosystems; *$p < 0.05$ vs. 10 µg/mL vs. corresponding DOX-loaded nanoparticles; **$p < 0.05$ vs. corresponding and same condition in MC3T3-E1 cells.

Table 1. Main properties of nanosystems synthetized in this work.

Material	MSN	MSN_{PAA}	MSN_{ConA}
Organic matter (TGA) (%)	4.5 ± 0.1	36.2 ± 0.7	46.5 ± 0.9
S_{BET} (m^2 g^{-1})	1210 ± 35	22 ± 1	12 ± 1
V_P (cm^3 g^{-1})	1.41 ± 0.03	0.11 ± 0.01	~ 0
D_P (nm)	2.4 ± 0.1	-	-
ζ-potential (mV)	-20.0 ± 1.0	-54.4 ± 4.0	-34.2 ± 0.5
Mean size (DLS) (nm)	180 ± 5	220 ± 8	260 ± 10